Phase transformation and superconducting properties of MgB_2 using ball-milled low purity boron

X. Xu, J. H. Kim, M. S. A. Hossain, J. S. Park, Y. Zhao, S. X. Dou, W. K. Yeoh, M. Rindfleisch, and M. Tomsic

---

Articles you may be interested in

Enhancement of the critical current density and flux pinning of MgB_2 superconductor by nanoparticle SiC doping
Applied Physics Letters **81**, 3419 (2002); 10.1063/1.1517398

Improved superconducting properties in nanocrystalline bulk MgB_2
Applied Physics Letters **80**, 2725 (2002); 10.1063/1.1469654

High critical current density of MgB_2 bulk superconductor doped with Ti and sintered at ambient pressure
Applied Physics Letters **79**, 1154 (2001); 10.1063/1.1396629

Touching the properties of NbTi by carbon doped tapes with mechanically alloyed MgB_2
Applied Physics Letters **91**, 082507 (2007); 10.1063/1.2773942

Carbohydrate doping to enhance electromagnetic properties of MgB_2 superconductors
Applied Physics Letters **89**, 142505 (2006); 10.1063/1.2358947

Universal relationship between crystallinity and irreversibility field of MgB_2
Applied Physics Letters **86**, 212502 (2005); 10.1063/1.1937991

Phase transformation and superconducting properties of MgB$_2$ using ball-milled low purity boron

X. Xu, J. H. Kim,[a)] M. S. A. Hossain, J. S. Park, Y. Zhao, and S. X. Dou
Institute for Superconducting and Electronic Materials, University of Wollongong, Wollongong, NSW 2522, Australia

W. K. Yeoh
IRC in Superconductivity and Department of Engineering, University of Cambridge, Madingley Road, Cambridge, CB3 0HE, United Kingdom

M. Rindfleisch and M. Tomsic
Hyper Tech Research, Inc., 1275 Kinnear Road, Columbus, Ohio 43212, USA

MgB$_2$ samples were prepared by using 96% boron (B) powder with strong crystalline phase that had been ball milled for various times. We observed samples that contained ball-milled 96% B in comparison with one made from as-supplied commercial 96% B, with the results showing a significant enhancement in the high field critical current density (J_c) due to small grain size and better reactivity. Specifically, many grain boundaries for MgB$_2$ could be acting as strong flux pinning centers. Based on Rowell connectivity analysis, when the ball-milling time increased, the connectivity factor, described as the active cross-sectional area fraction (A_F), was decreased. This implies that the intergrain connectivity became worse. These properties could lead to poor J_c in low field. However, the pinning force strength, $J_c^{1/2} \times B^{1/4}$, of samples using ball-milled 96% B is larger than that of the reference sample using commercial 96% B powder. These results accompany enhanced irreversibility (H_{irr}) and upper critical fields (H_{c2}). © *2008 American Institute of Physics.* [DOI: 10.1063/1.2832752]

I. INTRODUCTION

The discovery of the superconductivity of MgB$_2$ with a critical temperature (T_c) of 39 K has offered the promise of large scale and electronic device applications at approximately 20 K.[1] Specifically, the best self-field critical current density (J_c) of MgB$_2$ conductor fabricated by the powder-in-tube (PIT) method has passed 10^5 A cm^{-2} for operating temperatures up to 20 K. In the real market, nevertheless, the cost and performance of MgB$_2$ play a significant role in determining its value as a replacement for conventional conductors and other low and high temperature superconducting materials. For instance, MgB$_2$ conductor has a very low materials cost at \$0.20 m^{-1}, which translates into \$1.00 m^{-1} for finished strands and approximately \$1.00 kA^{-1} m^{-1} at 2 T and 4.2 K, based on a published report.[2] The natural abundances of Mg and B powders are also very great. Therefore, MgB$_2$ superconductor is one of the most promising candidates for magnet applications, when compared to Nb–Ti and Nb$_3$Sn, especially as its T_c of 39 K can be applied to a convenient cryogen-free magnet to work at an operating temperature of 15–20 K.

From the cost point of view, further, high grade (>99%) amorphous boron (B) powder is about 10 times more expensive than low grade (96%–97%) B powders, which contain some crystalline phase. Eventually, low purity starting materials are expected to have a great impact on the production economics, if the low purity B powders can be applied to produce commercial MgB$_2$ conductors. However, there are still considerable advantages in the 99% B, i.e., amorphous B with >99% grade has high reactivity compared to low grade 96% B, resulting in a decreased sintering temperature and increased J_c. To attain the desirable properties of 99% B, the properties of the low grade B powders, such as purity, size distribution, reactivity, particle size, etc., need to be well studied and systematically analyzed, as they can play an important role in determining the fundamental properties of the MgB$_2$.

It is thus necessary to study sample preparation processing to achieve good superconducting properties with low grade B powder. In our previous works, we reported an acid leaching process to purify the low grade B (Ref. 3) and the ball milling of the pure B powder (99%, amorphous), using different media such as acetone, ethanol, and toluene. All the processing led to enhancements in the critical current density (J_c) in high field.[4] There have also been reports from other groups using different ball-milling systems. For example, Gümbel *et al.*[5] attempted to fabricate nanostructured MgB$_2$ by mechanical alloying of elemental Mg and amorphous B powders in a planetary ball mill, followed by hot pressing at about 700 °C. They achieved a critical current density of $J_c \sim 1 \times 10^5$ A cm^{-2} at an applied field of 2.1 T and 20 K. Fang *et al.*[6] fabricated superconducting iron-clad MgB$_2$ tapes via the standard PIT process, using an ultrafine Mg and B mixture precursor prepared by high-energy ball milling. The critical current density achieved was 2.0×10^5 A cm^{-2} at 20 K and 0.6 T, and 1.1×10^5 A cm^{-2} in a 1.5 T magnetic field. Matsumoto *et al.*[7] also reported that ball milling Mg powder

a)Corresponding author: jhk@uow.edu.au.

for a short time is a very effective method of improving the J_c of tapes. Recently, Häßler and co-workers.[8–10] reported the best J_c result through pressure-assisted sintering using a mechanically alloyed precursor powder in pristine MgB_2 and nanostructured carbon-doped MgB_2. From their result,[8] it also places emphasis on the phase content, the density, and the superconducting properties of MgB_2 on the choice of B precursor powder. However, they only showed the effects of ball-milled Mg and Mg+B for MgB_2 superconductor. So, we need further systematic studies of ball-milling effects with the only low-grade B powder.

In this work, therefore, we evaluated the superconducting properties of MgB_2 made from low-grade B powder with a strong crystalline phase as a function of ball-milling time. We used low-grade 96% commercial B powder with strong crystalline phase as our reference sample. The lattice parameters, grain size, lattice strain, J_c, critical temperature (T_c), residual resistivity ratio (RRR), upper critical field (H_{c2}), irreversibility field (H_{irr}), and microstructures for MgB_2 using ball-milled B are presented in comparison with the reference sample.

II. EXPERIMENTAL DETAILS

MgB_2 pellets were prepared by an *in situ* reaction process. B powder (96%) with strong crystalline phase was prepared by ball milling, with toluene as the ball-milling medium. The ball-milling process was carried out for 4, 8, and 12 h at a rotation speed of 160 rpm. The powder to ball ratio was 1: 16 in a planetary ball-milling with agate jar and balls. The ball sizes used were 5 mm and 10 mm, respectively. And then these powders were dried in a vacuum oven to evaporate the toluene. Four kinds of B powders were prepared, including a powder with no ball milling: these are denoted as B96, BM4B96, BM8B96, and BM12B96, respectively. These powders were then mixed, ground, and pressed with the same Mg (99%) powder. All MgB_2 samples were sintered at 800 °C for 30 min under high purity argon (Ar >99.9%) gas. These MgB_2 samples are again identified as B96S, BM4B96S, BM8B96S, and BM12B96S, respectively. The heating rate was 5 °C min^{-1}. We also prepared the reference MgB_2 sample using 99% B for comparison.

The phase and crystal structure of all the samples were investigated by X-ray diffraction (XRD). The crystal structure was refined with the aid of the program Jade (ver. 5.0). T_c was defined as the onset temperature at which diamagnetic properties were observed. The magnetization was measured at 5 and 20 K using a Physical Properties Measurement System (PPMS, Quantum Design) in a time-varying magnetic field up to 8.5 T with a sweep rate of 50 Oe s^{-1}. All the samples for measurement were bar-shaped, with dimensions of $1 \times 2 \times 3$ mm^3. The magnetic J_c was derived from the width of the magnetization loop using Bean's model.[11] Transport measurements for resistivity (ρ) were done using a standard ac four-probe method. In addition, $H_{c2}(T)$ and $H_{irr}(T)$ were defined as the fields where the temperature-dependent resistance at constant magnetic field $R(H_{c2}, T)$ =$0.9R_{ns}$ and $R(H_{irr}, T)=0.1R_{ns}$, with R_{ns} being the normal state resistance near 40 K. The grain morphology and micro-
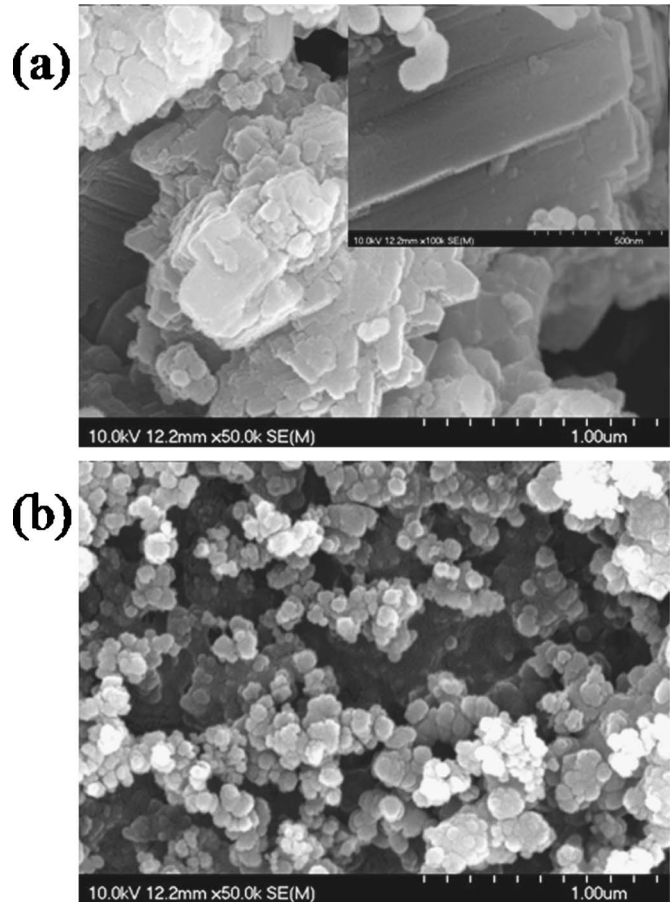

FIG. 1. Scanning electron microscope (SEM) images of (a) 96% B and (b) 99% B. Inset shows a high magnification image of 96% B.

structure were studied by scanning electron microscopy (SEM). The powder particle size and distribution were analyzed using a MASTERSIZER 2000 (ver. 3.01).

III. RESULTS AND DISCUSSION

Figure 1 shows SEM images for (a) 96% B and (b) 99% B powders. From the XRD results, we checked the phases of both powders in their initial state. It was observed that the particle size of the reference 99% B is smaller than that of the 96% B (indexed by B96). In addition, it shows better homogeneity, especially in the size distribution. The inset shows a high magnification image of the 96% B. It appears to show strong crystalline phase, which is not like the amorphous 99% B. All of these characteristics can influence the phase transformation of MgB_2 during sintering.

For the phase transformation of MgB_2 using 96% B and 99% B, differential thermal analysis was performed, and the results are shown in Fig. 2. The heating rate was 5 °C min^{-1} under flowing Ar, as with our sintering conditions. In both samples, there were two exothermal peaks. The first exothermal peak is due to the reaction between melted B_2O_3 and Mg. The B_2O_3 has no melting point, but rather a progressive softening and melting range from 300 to 700 °C under particular conditions.[12] The crystals begin to break down at 300 °C, and a series of suboxides are produced with partial melting until full fusion is reached at 700 °C. The main
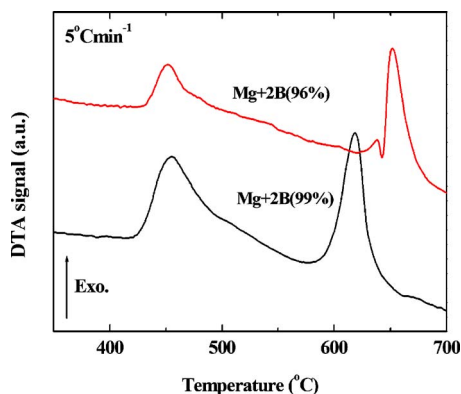
FIG. 2. (Color online) Differential thermal analysis for MgB_2 with different B powders.

reason for the presence of B_2O_3 in the B powder is because B has partially oxidized in air. As for the second exothermal peak, it can be attributed to the MgB_2 phase formation. What is interesting is that the second exothermal peaks of the two samples show different behavior. Specifically, the second exothermal peak of the sample using 96% B was slightly shifted to higher temperature, unlike sample using 99% B. In addition, there was a weak endothermal peak before the exothermal peak related to MgB_2 phase formation. This weak peak is related to the melting of Mg at around 650 °C. Using

96% B with crystalline phase can introduce shifting of the second exothermal peak. We conclude that phase formation of MgB_2 using 96% B with crystalline B can occur after Mg melting. This is because using B with crystalline phase requires more energy, due to poor reactivity between Mg and B.[13] This information was of importance in determining optimal sintering conditions for our samples. We speculate that the appropriate sintering temperature is above 650 °C for MgB_2 using 96% B, and in particular, above the Mg melting point. Note that the first exothermal peak did not shift to higher temperature. If this peak is related to the solid–solid reaction of MgB_2, this also should be shifted to a higher temperature because of the different crystallinity.

To improve the reactivity between Mg and 96% B with crystalline phase, we tried to ball mill the B powder by itself. This is because Mg handing is relatively difficult due to its easy oxidation, even Ar atmosphere. SEM images as a function of ball milling time are shown in Fig. 3. It was observed that the average particle size of the reference B96 was approximately 200 nm, whereas ball-milled B96 was in the size range of 150–170 nm. Even when the ball-milling time was significantly increased to 12 h, the particle size did not show any significant differences in our ball-milled B96 powders. However, it seems to become more homogeneous with increasing ball-milling time. These results are further confirmed by the size distributions of particles in Fig. 4. From
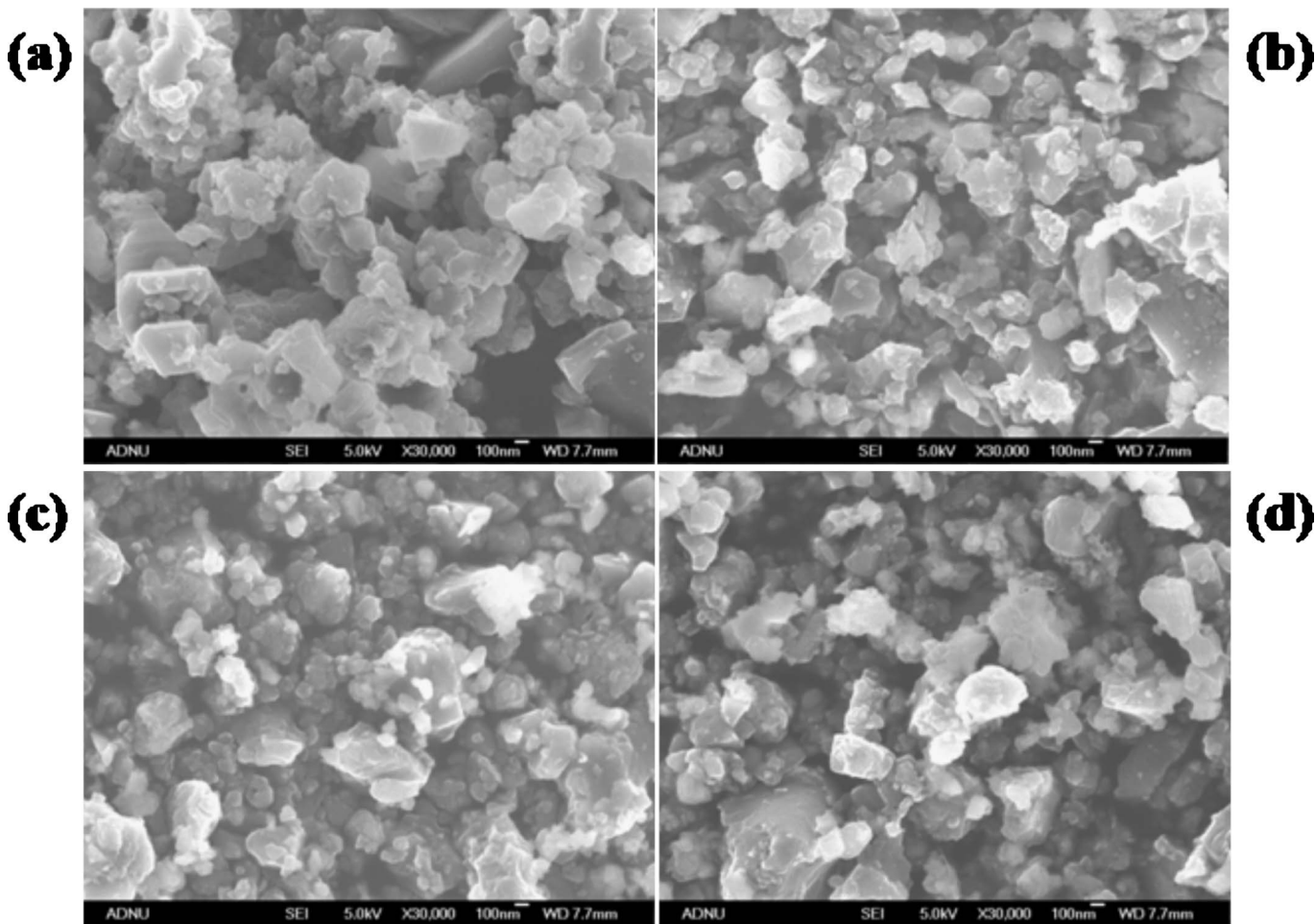

FIG. 3. Scanning electron microscope (SEM) images for (a) B96, (b) BM4B96, (c) BM8B96, and (d) BM12B96.
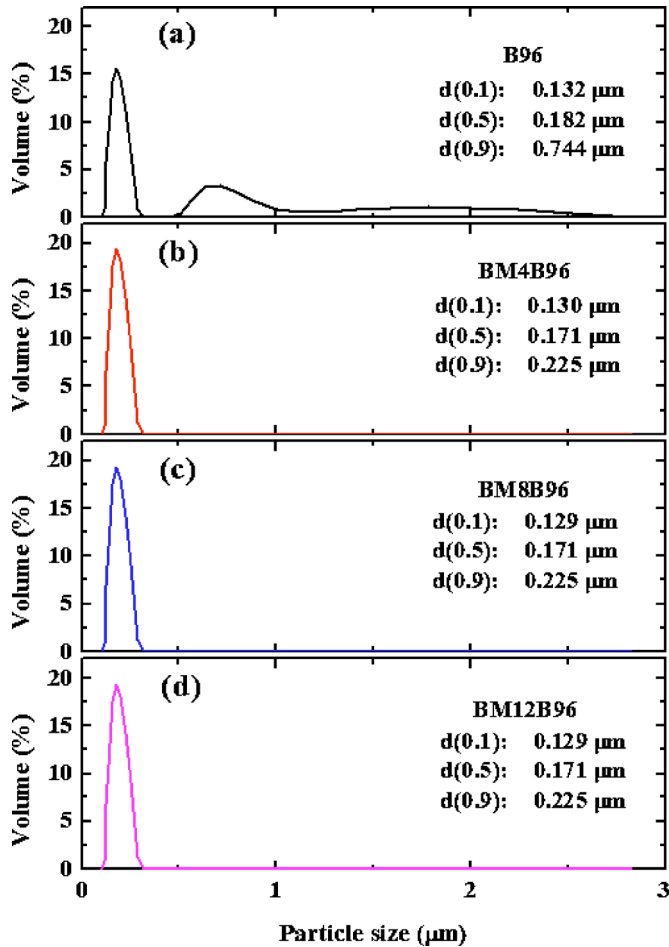
FIG. 4. (Color online) Particle size distribution for (a) B96, (b) BM4B96, (c) BM8B96, and (d) BM12B96.

FIG. 5. (Color online) (a) a- and c-axis lattice parameters, (b) c/a, (c) full-width at half-maximum (FWHM) of the (110) peak, and (d) lattice strain of MgB$_2$ samples using different B.

the results, it can be seen that there was bimodal behavior before ball-mill processing. That is to say, after ball milling, the B96 particles with sizes between 500 and 2500 nm disappeared. The agglomerated B powders were homogeneously dispersed. Obviously, the results of particle size measurements show identical results for the ball-milled powders. It is well known that such particle size measurements strongly depend on the agglomeration of the powder. However, it should be unlikely that increasing the milling time by 100% or more do not give further reductions of particle size. As a result, the ball-milled B can improve the reactivity. The smaller particle size and greater homogeneity leads to the vies that the MgB$_2$ particle size was determined by the size of the B powder during the sintering process, so this result must affect the superconducting properties of the samples that were formed from these B powders.

Figure 5 shows the estimated results (from XRD) for MgB$_2$ superconductor made from B with different ball-milling times. We observed that lattice constants such as the a- and c-axis parameters did not change within the accuracy of error. However, the c/a value, which is related to structure volume, was a little decreased. This behavior can be related to the distortion of the lattice due to the storage of energy through ball milling. Even though we used a medium that contained carbon (C) in our experimental procedure, there were no apparent C substitution effects among the samples.
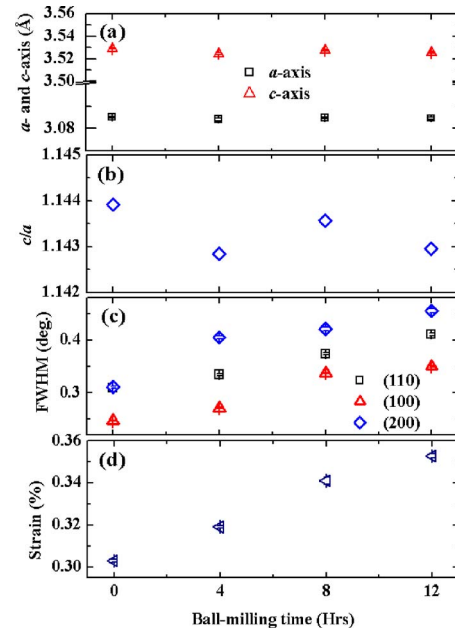
At least, the doping level of C is almost the same within a 12 h ball-milling time. According to the results of Avdeev *et al.*,[14] the level of C substitution, x in the formula Mg(B$_{1-x}$C$_x$)$_2$. can be estimated as $x = 7.5\Delta(c/a)$, where $\Delta(c/a)$ is the change in c/a compared to a pure sample. Estimated value for all samples was ~ 0.005 in the composition of Mg(B$_{1-x}$C$_x$)$_2$. However, the c/a value is also depended on lattice distortion due to crystallinity, as mentioned earlier. In general, ball-milling processing leads to poorer crystallinity and connectivity of MgB$_2$. Finally, these can affect the full-width at half-maximum (FWHM) of diffractions. In our experiment, the ball milling affects the broadening of the FWHM of the characteristic MgB$_2$ peaks for sintered MgB$_2$ samples. This again indicates that crystallinity has become poorer. It is well known that the sorts of peak broadening reflected by the FWHM values can be caused by both crystalline size and lattice strain. In particular, the effects of the crystalline size of B powder can be attributed to the grain size of MgB$_2$. From the lattice defect point of view, again, the degradation of the crystallinity for MgB$_2$ originates from disordered crystal lattice that is caused by ball milling. As can be seen in Fig. 5, the calculated FWHM values of the (110) peak were 0.309°, 0.334°, 0.374°, and 0.511°, respectively, for 0, 4, 8, and 12 h of ball milling. The (100) and (002) peaks also showed the same trends. The T_c values decreased from 37.6 to 36.4 K as the ball milling time increased to 12 h. The behavior of T_c had an opposite trend from the FWHM.

It should be noted that the relative MgO intensity, MgO(220)/MgB$_2$(110)+MgB$_2$(102)(%), increased with increasing ball-milling time, as is shown in Fig. 6. Even though there was no oxygen (O) content in the toluene, ball milling and evaporation processing can introduce some O content, indicating the easy oxidation of B powder. Usually, B$_2$O$_3$ peaks ($2\theta \sim 14.6°$ and $27.8°$) appeared in the ball-
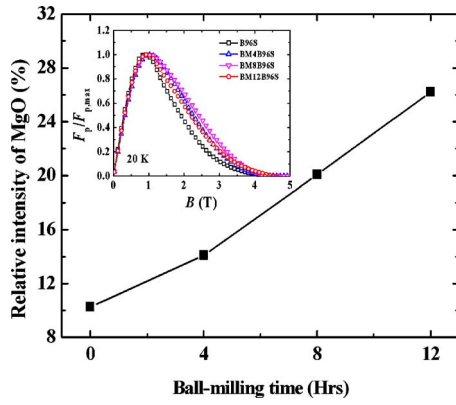
FIG. 6. (Color online) Relative intensity, $MgO(220)/MgB_2(110)$ $+MgB_2(102)$, as a function of ball-milling time. (Inset) Relative pinning force as a function of field for the different samples.

FIG. 7. (Color online) The magnetic critical current density (J_c) for all MgB_2 samples as a function of external magnetic field at 5 and 20 K.

milled B powders. What is the key point is that the storage of energy in the B powder is increased through ball milling. This can improve the reactivity between Mg and B, on the other hand, this makes the reaction between B and O much easier during the mixing process. That is to say, even though there was crystalline phase in low grade B powder, ball-mill processing can induce greater reactivity between Mg and B powders. In addition, the oxide layer on the B surfaces was probably broken during ball milling. It is well known that an increased MgO fraction affects the degradation of superconductivity. The MgO nanoparticles could, however, enhance the flux pinning effects according to two-gap superconductivity theory. As the coherence length $\xi^{ab}(0)$ of MgB_2 is approximately 6–7 nm, inclusion of MgO particles ($\sim$20 nm) within grains could result in strong flux pinning centers. However, the presence of excess oxide phases or large-sized particles ($>$50 nm) at the grain boundaries could result in degradation of grain connectivity. For superconductivity, therefore, MgO as the main secondary phase will be of great importance and yield a positive or negative effect for the J_c at the same time. If oxidation results in the presence of MgO, it also causes Mg deficiency. The presence of Mg vacancies in the MgB_2 structure could be responsible for the change in the structural volume of our ball-milled samples and cause the significant degradation of T_c. Even though ball-mill processing still has a lot of disadvantages for MgB_2, this can also introduce small grain size after sintering, resulting in strong flux pinning centers, as can be seen in the inset of Fig. 6. As a result, we need to study the correlation between MgO formation and flux pinning.

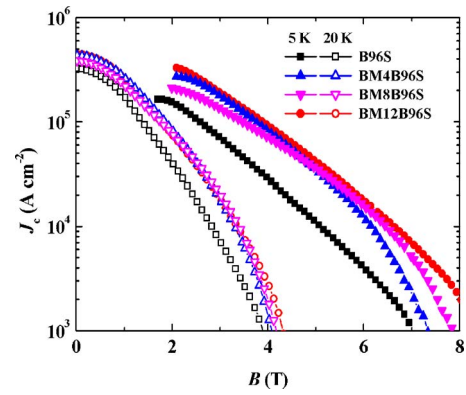To further understand the positive or negative effects of

MgO particles in our samples, the dependence of the resistivity (ρ) of MgB_2 on the use of different ball-milled B powders, can be seen in Table I, where resistivity values at 40 and 300 K increased as the B ball-milling time increased. Specifically, a lower value of ρ at 300 K indicates good grain connectivity. This can be further supported by the RRR ($\rho_{300\ K}/\rho_{40\ K}$) values. The RRR values decreased from 2.65 to 1.86, as the ball-milling time increased. Rowell[15] also reported that $\Delta\rho$ ($\rho_{300\ K}-\rho_{40\ K}$) is of great importance for estimating the grain connectivity. According to the Rowell connectivity analysis, the active cross-sectional area fraction (A_F) represents the connectivity, which is estimated by comparing the measured value with that of a single crystal. Although $\Delta\rho$ of Rowell[15] and Jiang *et al.*[16] assumed 4.3 and 7.3 $\mu\Omega$ cm, respectively, with different reference values, we can show that the behavior varies with different ball-milling times. The data can explain the connectivity effects on ball-milled samples, that when the ball-milling time is increasing, the grain connectivity becomes worse, leading to no obvious differences in J_c in low field at 20 K, but large improvements for the ball-milled samples in high field at 5 K, as shown in Fig. 7.

Currently in the literature, Matsumoto *et al.*[7] have reported that ball milling Mg alone enhanced the J_c. However, ball-milled MgH_2 as a precursor did not result in increased J_c value. The presence of light MgO particles due to ball milling may be effective for high J_c. On the other hand, MgO acts as a current barrier in MgB_2,[16] causing decreased active area fraction and increased resistivity, while having various effects on the grain connectivity, so as to reduce the J_c in low field. Clearly, the formation possibilities for MgO within

TABLE I. Measured resistivity values, residual resistivity ratios (RRR), and active cross-sectional area fraction (A_F) for MgB_2 with different ball-milling times.

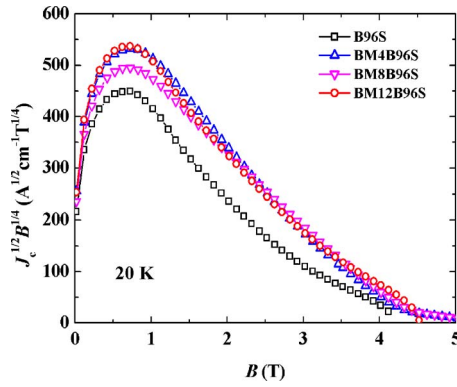| Samples	$\rho_{40\ K}$ ($\mu\Omega$ cm)	$\rho_{300\ K}$ ($\mu\Omega$ cm)	$\Delta\rho$ ($\rho_{300\ K}-\rho_{40\ K}$) ($\mu\Omega$ cm)	RRR	A_F	T_c (K)
B96S	13.4	35.7	22.3	2.66	0.33	37.6
BM4B96S	19.6	42.6	23.0	2.18	0.32	37.0
BM8B96S	29.8	54.5	24.7	1.83	0.29	36.3
BM12B96S	66.8	124.3	57.5	1.86	0.13	36.4

FIG. 8. (Color online) Kramer plot (F_k) of the pinning force, $J_c^{1/2} \times B^{1/4}$, for all samples at 20 K.

MgB_2 exist because Mg can act as a potential O getter in air or because of oxidation during sintering due to gaseous O.

Figure 7 shows the magnetic $J_c(B)$ behavior at 5 and 20 K. At 5 K, J_c for the sample with 12 h ball-milled B was estimated to be 2000 A cm^{-2} at 8 T. This J_c value is much higher than for the sample without any ball-milling process. This is due to the small grain size, which is effective for enhancing flux pinning. However, the difference in the J_c became smaller under low field, <2 T. On the other hand, $J_c(B)$ behavior at 20 K did not exhibit much difference. This is because the T_c of the samples affected $J_c(B)$. In addition, grain boundary effects were negligible. For example, even though the samples using ball-milled B had good $J_c(B)$ performance at 5 K and 4 T, $J_c(B)$ for all samples showed little difference at 20 K and 4 T. That is, grain connectivity or high T_c of samples is of great importance at 20 K. What is interesting is that self-field J_c remained unchanged after ball milling. Further work is needed to clarify this issue.

These phenomena can further be supported by the Kramer plot (F_k) (Ref. 17) at 20 K, as can be seen in Fig. 8. Pinning force strength, $J_c^{1/2} \times B^{1/4}$, is a linear function of magnetic field (B). It was observed that the pinning force of all the ball-milled samples is larger than that of the reference sample. The improved pinning in field seems to be caused by the enhanced grain boundary pinning provided by the larger number of grain boundaries. Although F_k is not really linear at low field, if we extrapolate F_k to zero, we can deduce the characteristic H_{irr} values. The main reason for the curvature at lower J_c might be due to percolative paths, which in fact give a transport J_c that is always higher than the value extracted from magnetic loop.[18]

From $R-T$ curve, the temperature dependence of H_{irr} and H_{c2} for all the samples is shown in Fig. 9. As can be seen in Fig. 9, the values of H_{c2} and H_{irr} were enhanced systematically as the ball-milling time increased to 12 h. These properties showed the same trends as $J_c(B)$ at 5 K. This indicates that degradation of crystallinity is the guiding principle for high H_{irr} and H_{c2}. In addition, the $H_{c2}-T$ curves of all samples show similar behavior to those of $H_{irr}-T$. For example, the curves showed a positive curvature very near T_c, whereas the curve was linear except for this region. The positive curvature of H_{c2} at $T \approx T_c$ indicates that the diffusivity in the σ bands is suppressed compared to that in the π bands.[19]
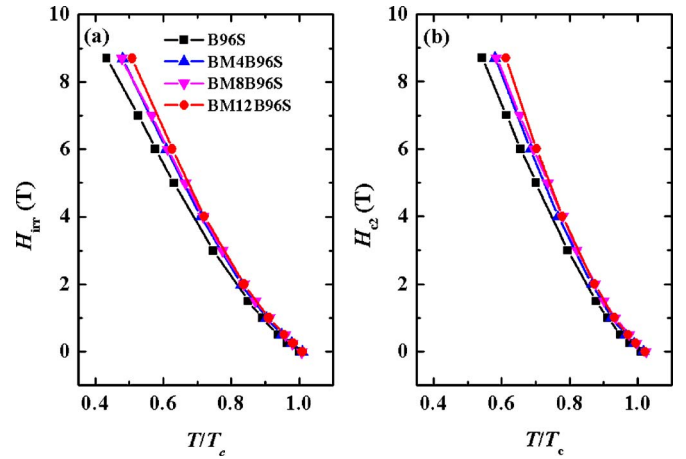

FIG. 9. (Color online) Temperature dependence of irreversibility field (H_{irr}) and upper critical field (H_{c2}) for all samples with different ball-milling times.

IV. SUMMARY

In conclusion, we have shown that the starting B powder is important in determining the $J_c(B)$ performance of MgB_2 samples. The reactivity of 96% B powder can be improved by using ball-mill processing, leading to enhanced magnetic critical current density, J_c, compared to the original 96% B powder. The A_F values can explain the connectivity effects on ball-milled samples; when the ball-milling time is increased, the grain connectivity becomes worse, leading to little change in J_c in low field at 20 K, but strong effects on the high field J_c at 5 K. This could be related to the small grain size and poor crystallinity. Specifically, the MgO fraction was increased within the matrix through ball milling, which influences properties such as flux pinning. Further study of the ball-milling process thus promises to allow adjustment of the desired phase form, which should be optimized along with the sintering conditions, so as to create a balance between the intergrain connectivity and the pinning centers. We should also rethink the possibilities of metal-oxide dopants in MgB_2 to obtain possible enhancements to the superconductivity. The MgB_2 made using low grade 96% B powder could be particularly useful for industrial applications because of its low material cost.

[1] J. Nagamatsu, N. Nakagawa, T. Muranaka, Y. Zenitani, and J. Akimitsu, Nature (London) **410**, 63 (2001).
[2] L. D. Cooley, A. K. Ghosh, and R. M. Scanlan, Supercond. Sci. Technol. **18**, R51 (2005).
[3] X. Xu, M. J. Qin, K. Konstantinov, D. Dos Santos, W. K. Yeoh, J. H. Kim, and S. X. Dou, Supercond. Sci. Technol. **19**, 466 (2006).
[4] X. Xu, J. H. Kim, W. K. Yeoh, Y. Zhang, and S. X. Dou, Supercond. Sci. Technol. **19**, L47 (2006).

[5]A. Gümbel, J. Eckert, G. Fuchs, K. Nenkov, K.-H. Muller, and L. Schultz, Appl. Phys. Lett. **80**, 2725 (2002).

[6]H. Fang, S. Padmanabhan, Y. X. Zhou, and K. Salama, Appl. Phys. Lett. **82**, 4113 (2003).

[7]A. Matsumoto, H. Kumakura, H. Kitaguchi, H. Hatakeyama, H. Yamada, and M. Hirakawa, IEEE Trans. Appl. Supercond. **15**, 3333 (2005).

[8]W. Häßler, B. Birajdar, W. Gruner, M. Herrmann, O. Perner, C. Rodig, M. Schubert, B. Holzapfel, O. Eible, and L. Schultz, Supercond. Sci. Technol. **19**, 512 (2006).

[9]M. Herrmann, W. Häßler, C. Mickel, W. Gruner, B. Holzapfel, and L. Schultz, Supercond. Sci. Technol. **20**, 1108 (2007).

[10]M. Herrmann, W. Häßler, C. Rodig, W. Gruner, B. Holzapfel, and L. Schultz, Appl. Phys. Lett. **91**, 082507 (2007).

[11]C. P. Bean, Rev. Mod. Phys. **36**, 31 (1964).

[12]J. H. Kim, S. X. Dou, D. Q. Shi, M. Rindfleisch, and M. Tomsic, Supercond. Sci. Technol. **20**, 1026 (2007).

[13]S. K. Chen, K. A. Yates, M. G. Blamire, and J. L. MacManus-Driscoll, Supercond. Sci. Technol. **18**, 1473 (2005).

[14]M. Avdeev, J. D. Jorgensen, R. A. Ribeiro, S. L. Bud'ko, and P. C. Canfield, Physica C **387**, 301 (2003).

[15]J. M. Rowell, Supercond. Sci. Technol. **16**, R17 (2003).

[16]J. Jiang, B. J. Senkowicz, D. C. Larbalestier, and E. E. Hellstrom, Supercond. Sci. Technol. **19**, L33 (2006).

[17]E. J. Kramer, J. Appl. Phys. **44**, 1360 (1973).

[18]V. Braccini, L. D. Cooley, S. Patnaik, D. C. Labalestier, P. Manfrenetti, A. Palenzona, and A. S. Siri, Appl. Phys. Lett. **81**, 4577 (2002).

[19]A. Gurevich, Phys. Rev. B **67**, 184515 (2003).